Cavity optomechanical detection of persistent currents and solitons in a bosonic ring condensate

Nalinikanta Pradhan [1], Pardeep Kumar [2,*], Rina Kanamoto [3], Tarak Nath Dey [1], M. Bhattacharya [4] and Pankaj Kumar Mishra [1]

[1] *Department of Physics, Indian Institute of Technology, Guwahati 781039, Assam, India*
[2] *Max Planck Institute for the Science of Light, Staudtstraße 2, 91058 Erlangen, Germany*
[3] *Department of Physics, Meiji University, Kawasaki, Kanagawa 214-8571, Japan*
[4] *School of Physics and Astronomy, Rochester Institute of Technology, 84 Lomb Memorial Drive, Rochester, New York 14623, USA*

(Received 12 June 2023; accepted 8 January 2024; published 26 January 2024)

We present numerical simulations of the cavity optomechanical detection of persistent currents and bright solitons in an atomic Bose-Einstein condensate confined in a ring trap. This paper describes a technique that measures condensate rotation *in situ*, in real time, and with minimal destruction, in contrast to currently used methods, all of which destroy the condensate completely. For weakly repulsive interatomic interactions, the analysis of persistent currents extends our previous few-mode treatment of the condensate [P. Kumar *et al.* Phys. Rev. Lett. **127**, 113601 (2021)] to a stochastic Gross-Pitaevskii simulation. For weakly attractive atomic interactions, we present the first analysis of optomechanical detection of matter-wave soliton motion. We provide optical cavity transmission spectra containing signatures of the condensate rotation, sensitivity as a function of the system response frequency, and atomic density profiles quantifying the effect of the measurement backaction on the condensate. We treat the atoms at a mean-field level and the optical field classically, account for damping and noise in both degrees of freedom, and investigate the linear as well as nonlinear response of the configuration. Our results are consequential for the characterization of rotating matter waves in studies of atomtronics, superfluid hydrodynamics, and matter-wave soliton interferometry.

DOI: 10.1103/PhysRevResearch.6.013104

I. INTRODUCTION

An atomic Bose-Einstein condensate (BEC) confined in a ring potential exhibits superflow, i.e., transport without dissipation [1–3]. It is therefore a natural platform for studying superfluid hydrodynamical phenomena such as quantized persistent currents [4], phase slips [5,6], excitations [7], two-component rotation [8,9], hysteresis [10,11], and shock waves [12]; a versatile enabler for applications such as matter-wave interferometry [13,14], atomtronic circuits [15–18], and gyroscopy [19,20]; and a convenient simulator of topological excitations [21–23], early universe cosmology [24], and time crystals [25].

Inspired by the experimental activity in the field, a large number of theoretical proposals have been put forward, based on the BEC-in-a-ring system, characterizing plain wave to soliton transitions [26], self-trapping [27], simulation of Hawking radiation [28], the Berry phase [29], qubits for computation [30], critical velocities [31,32], superflow decay [33–36], phonon detection in a toroidal BEC [37], rotating lattices [38], rotation sensing [39], the effect of gauge fields [40], matter-wave interference [41], double-ring geometries [42–44], existence of persistent currents with nonquantized angular momentum [45], etc.

In all these studies, knowledge of the condensate rotation is an important consideration. At present, all demonstrated methods of detecting such rotation in ring BECs are destructive of the condensate [46]. Due to issues related to optical resolution, the methods typically also require time-of-flight expansion of the atoms, making *in situ* measurements difficult. A theoretical proposal exists based on atom counting for a minimally destructive measurement of the condensate rotation [47].

Recently, our group suggested a method for detecting condensate rotation in real time, *in situ*, and with minimal destruction to the condensate [48]. This method proposed to use the techniques of cavity optomechanics, a discipline that addresses the coupling of mechanical motion to electromagnetic fields confined in resonators [49]. Probably the best-known optomechanical device in existence is the Laser Interferometer Gravitational-Wave Observatory, which detected the gravitational waves predicted by Einstein's theory of general relativity, an accomplishment recognized by a Nobel prize [50]. The minimally destructive measurement in our case relied on the optomechanical coupling based on the dispersive light-matter interaction [49].

Cavity optomechanics is now a mature field that is capable of supporting the sensitive detection of any physical variable that actuates the mechanical motion coupling to the electromagnetic fields in the cavity. Thus, cavity optomechanical principles have been employed to construct accelerometers [51], magnetometers [52], thermometers [53], mass [54] and

*Corresponding author: pardeep.kumar@mpl.mpg.de

force [55,56] sensors, etc. In our previous proposal, which considered a rotating BEC in a cavity, it was shown that the resulting sensitivity of BEC rotation measurement was three orders of magnitude better than demonstrated hitherto [48]. This conclusion regarding the detection of a persistent current was based on a few-mode approximation for the condensate.

In the present paper, we consider a BEC confined in a ring trap and interacting with an optical cavity mode carrying orbital angular momentum (OAM) [48]. This may be regarded as the rotational analog of a BEC with a linear degree of mechanical freedom combined with a standing wave optical cavity lattice in an optomechanical context which has been realized experimentally [57].

For weak repulsive atomic interactions, we extend the previous two-mode characterization of the condensate to a mean field, i.e., Gross-Pitaevskii, treatment. Our method allows us to confirm the basic results of the two-mode treatment regarding the rotation detection of a persistent current, to investigate the modifications resulting from taking the full condensate dynamics into account, and to quantify the effect of measurement backaction on the condensate. It also allows us to consider the detection of a superposition of persistent current states in the condensate.

We also investigate the case of weak attractive atomic interactions [58]—which results in a bright-soliton ground state in the ring condensate—in the optomechanical context. Such solitons are of great interest, e.g., to rotation sensing and matter-wave interferometry [59–65]. However, a soliton is not amenable to a few-mode optomechanical treatment due to the large number of matter-wave OAM states contributing to the condensate dynamics. Our numerical simulations make this case tractable, extracting, as in the case of the persistent currents, cavity transmission spectra with signatures of soliton rotation, the sensitivity of the measurement as a function of system response frequency, and atomic density profiles showing the effect of the measurement on the condensate. In all simulations, the matter is treated at the mean-field level, light is treated classically, and noise arising from both optical as well as matter-wave fields are taken into account.

This paper is organized as follows. In Sec. II, the theoretical model and details of the numerical simulation are presented. In Sec. III, we provide the dynamics, OAM content, optical spectra, measurement sensitivity, and condensate density fidelity for the persistent current and bright soliton detection, respectively. The conclusions are presented in Sec. IV. Appendix A summarizes our theoretical model and Appendix B presents results at higher optical power.

II. THEORETICAL MODEL AND DETAILS OF NUMERICAL SIMULATION

In this section, we present the theoretical model for the configuration of interest, shown in Fig. 1, i.e., a BEC confined in a one-dimensional ring trap coupled to a cavity using Laguerre-Gauss beams [48]. The coupling of a harmonically trapped, simply connected, BEC to an optical cavity has been realized experimentally [57]. Ring BECs have separately been realized in other experiments [1,4,5] and may be readily combined with optical modes carrying OAM in cavities [66].

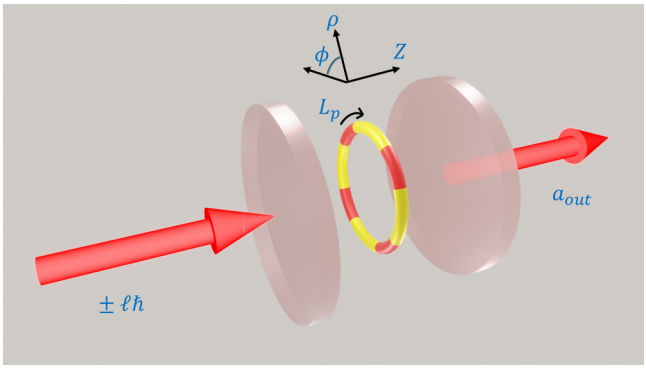

FIG. 1. A schematic setup for the BEC with winding number L_p rotating in a ring trap around the axis of the Fabry-Perot cavity. The red beam represents the Laguerre-Gauss modes with the orbital angular momentum of $\pm\ell\hbar$ used to probe the BEC rotation. The output signal $a_{\rm out}$ is the field transmitted from the cavity.

The dynamical equations governing the system are given by [48,57,67–69]

$$(i-\Gamma)\frac{d\psi}{d\tau} = \Big[-\frac{d^2}{d\phi^2} + \frac{U_0}{\omega_\beta}|\alpha(\tau)|^2\cos^2(\ell\phi) - \mu + 2\pi\frac{\chi}{N}|\psi|^2\Big]\psi + \xi(\phi,\tau) \tag{1}$$

and

$$i\frac{d\alpha}{d\tau} = \Big\{-\Big[\Delta_c - U_0\langle\cos^2(\ell\phi)\rangle_\tau + i\frac{\gamma_0}{2}\Big]\alpha + i\eta\Big\}\omega_\beta^{-1} + i\sqrt{\gamma_0}\omega_\beta^{-1}\alpha_{\rm in}(\tau). \tag{2}$$

In the above, Eq. (1) is the stochastic Gross-Pitaevskii equation, where $\psi \equiv \psi(\phi,\tau)$ represents the microscopic wave function of the condensate with ϕ the angular variable along the ring and τ the scaled time, to be defined below. The wave function obeys, at any time, the normalization condition

$$\int_0^{2\pi} |\psi(\phi,\tau)|^2 d\phi = N,$$

where N is the number of atoms in the condensate. To obtain the dimensionless Eq. (1), the energy and time have been scaled using the quantities

$$\hbar\omega_\beta = \frac{\hbar^2}{2mR^2} \text{ and } \tau = \omega_\beta t, \tag{3}$$

respectively, where m is the atomic mass and R is the radius of the ring-shaped trap.

The first term inside the square bracket on the right-hand side of Eq. (1) stands for the kinetic energy of the atoms due to their rotational motion. The second term in the bracket represents the optical lattice potential created with a superposition of two Laguerre-Gauss beams having orbital angular momenta $\pm\ell\hbar$, respectively, with $U_0 = g_0^2/\Delta_a$, where g_0 is the single photon-single atom coupling and Δ_a is the detuning of the driving laser from the atomic resonance. The third term in the bracket corresponds to the chemical potential μ of the condensate, which is corrected by $\Delta\mu$ at each time step $(\Delta\tau)$

as [70]

$$\Delta\mu = (\Delta\tau)^{-1} \ln\left[\int |\psi(\phi,\tau)|^2 d\phi \Big/ \int |\psi(\phi,\tau+\Delta\tau)|^2 d\phi\right]$$

to conserve the normalization of the condensate in the presence of the dissipation

$$\Gamma = \frac{\omega_m}{\omega_\beta}, \tag{4}$$

set by the lifetime ω_m^{-1} of the persistent currents [1,48]. The fourth term inside the bracket represents the scaled atomic interaction:

$$\chi = \frac{gN}{2\pi\hbar\omega_\beta}. \tag{5}$$

Here

$$g = \frac{2\hbar\omega_\rho a_s}{R}, \tag{6}$$

with a_s the s-wave atomic scattering length and ω_ρ the harmonic trap frequency along the radial direction [48]. Thermal noise ξ, with zero mean and correlations provided below, has been added to the condensate in accordance with fluctuation-dissipation theory [71].

The dynamics of the complex intracavity coherent field amplitude α is described by Eq. (2). In our simulations, we have treated α as a classical quantity, as this approximation has been shown to be adequate for similar setups experimentally. For example, in Ref. [57], although bistability is observed at intracavity photon numbers below unity ($|\alpha|^2 \lesssim 1$), the corresponding experimental data is very well described using a classical theory for the optical field [72]. As explained in Ref. [73], this is due to the fact that in the bad cavity limit [49], where the condensate mechanical (i.e., side mode) oscillation frequencies are smaller than the cavity linewidth, the number of photons passing through the cavity during one mechanical period is much larger than one. The quantum fluctuations in the photon number thus have a negligible effect on the dynamics of the condensate density modulations. In our simulations below, we have ensured that the bad cavity limit always applies.

In the first term inside the square bracket on the right-hand side of Eq. (2), Δ_c signifies the detuning of the driving field frequency from the cavity resonance frequency ω_c. The second term represents the coupling between the light mode and condensate, where the expectation value of the light potential $\cos^2(\ell\phi)$ taken with respect to the condensate wave function $\psi(\phi,\tau)$,

$$\langle\cos^2(\ell\phi)\rangle_\tau = \int_0^{2\pi} |\psi(\phi,\tau)|^2 \cos^2(\ell\phi) d\phi, \tag{7}$$

is a time-dependent quantity. In the third term, γ_0 is the energy decay rate of the cavity field. The last term inside the curly braces represents the laser drive with pump rate $\eta = \sqrt{P_{\rm in}\gamma_0/\hbar\omega_c}$, where $P_{\rm in}$ is the input optical power. The last term on the right-hand side of Eq. (2) signifies the optical shot noise present in the system. The thermal and optical fluctuations each have zero mean and their correlations are given by [22,48]

$$\langle\xi(\phi,\tau)\xi^*(\phi',\tau')\rangle = 2\Gamma T\,\delta(\phi-\phi')\,\delta(\tau-\tau'), \tag{8}$$

$$\langle\alpha_{\rm in}(\tau)\,\alpha_{\rm in}^*(\tau')\rangle = \omega_\beta\,\delta(\tau-\tau'), \tag{9}$$

where T is the nondimensionalized temperature in units of $k_B/(\hbar\omega_\beta)$, with k_B being the Boltzmann constant. For the numerical simulation of these stochastic equations, the noise terms are modeled as follows:

$$\xi(\phi,\tau) = \sqrt{2\Gamma T/(d\phi\,d\tau)}\,\mathcal{N}(0,1,N_\phi)\,\mathcal{N}(0,1,N_\phi), \tag{10}$$

$$\alpha_{\rm in}(\tau) = \sqrt{\omega_\beta/d\tau}\,\mathcal{N}(0,1,1), \tag{11}$$

where $\mathcal{N}(0,1,N_\phi)$ is a set of N_ϕ random numbers that are normally distributed with zero mean and unit variance and N_ϕ is the number of grid points along the ϕ direction. Two sets of random numbers are being multiplied in $\xi(\phi,\tau)$ to capture the inherent randomness of the condensate wave function across both spatial and temporal dimensions. We have considered $N_\phi = 1024$ for all simulations. The term $\mathcal{N}(0,1,1)$ in Eq. (11) corresponds to a single random number, drawn from a normal distribution having a zero mean and unit variance.

To attain the dynamics of the persistent current, we have considered the initial state as a plane wave and then evolved the system in real-time using the coupled BEC-cavity equations and the Runge-Kutta fourth-order (RK4) scheme [74]. A different approach is taken for the case of the soliton. Initially, we prepare a localized state with a Gaussian density profile, and then we evolve it in imaginary time using the Strang splitting Fourier method [75] to reach a soliton as its ground state in the presence of an optical lattice as well as atomic interactions. The resulting ground state is then used as the initial state for the subsequent real-time evolution using the RK4 scheme. We simulate a single trajectory of the cavity field and condensate wave function over a duration of five seconds, which is sufficiently long to capture the relevant dynamics of the system. By applying a moving average of 30 Hz to the cavity output spectrum, we obtain results that are comparable to the ensemble average over multiple trajectories. We have adopted the time step $d\tau = 10^{-7}$ for all simulations.

In this paper, we have considered the parameters that are readily realizable in the experiment. We have utilized the fact that BECs with cavities [57], ring BECs [1], and cavities with OAM-carrying modes [66] have already been implemented in the laboratory. On similar lines, the bound state cases like solitons considered in the paper have been launched into the magnetic waveguides, in which the ring trap could be considered as a variation. As the methodology adopted in the paper mainly considers the combination of the above-mentioned different experimental setups, for the ease of the readers, wherever required we have provided the parameters taken from the relevant experiments for our simulations.

III. RESULTS

A. Persistent currents

1. Rotational eigenstate

In this section, we present the dynamics accompanying the detection of a persistent current in the ring BEC. Such currents can exist for macroscopic times as metastable flow states of

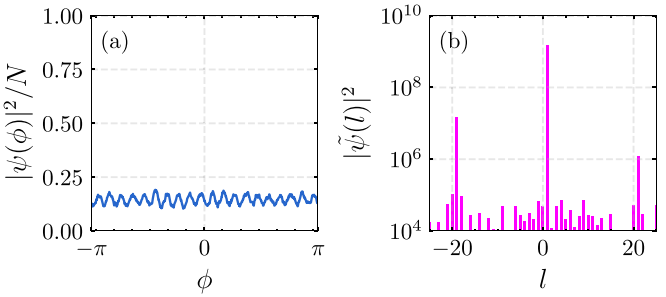

FIG. 2. (a) Angular profile of the condensate density per particle for a persistent current rotational eigenstate (b) OAM state content of the condensate. Parameters used here are $\Gamma = 0.0001$, $T = 10$ nK $\times k_B/(\hbar\omega_\beta)$, $g/\hbar \simeq 2\pi \times 0.02$ Hz, $L_p = 1$, $\ell = 10$, $N = 10^4$, $\tilde{\Delta} = -2\pi \times 173$ Hz, $U_0 = 2\pi \times 212$ Hz, $\gamma_0 = 2\pi \times 2$ MHz, $P_{\rm in} = 0.2$ pW, $\omega_c = 2\pi \times 10^{15}$ Hz, $m = 23$ amu, and $R = 12$ μm [1,57].

the condensate with atoms that weakly repel each other [1]. The basic idea is for the circular optical lattice to act as a probe of the angular momentum, and hence the winding number, of the condensate [48]. For low intracavity photon numbers, the matter wave Bragg diffracts from the weak optical lattice. This results, in the first order, in two additional OAM states (side modes), which modulate the condensate density. These modulations add sidebands to the optical modes, which can subsequently be detected in the cavity transmission.

In our simulation, for which we have used ^{23}Na atoms [1], a phase gradient is imprinted initially on the condensate to impart a winding number L_p to it. The resulting persistent current then gets coupled to the angular optical lattice, which displays 2ℓ interference maxima along the ring, on which the BEC is trapped.

For all our simulations related to the persistent current, we consider an initial state for the condensate wave function of the form

$$\psi(\phi) = \sqrt{\frac{N}{2\pi}} e^{iL_p\phi}, \tag{12}$$

which corresponds to an eigenstate of condensate rotation in the absence of the optical lattice, with L_p being the winding number of the condensate. In writing Eq. (12), we have assumed that the temperature of the BEC is far below its critical value, so the thermal fraction is negligible; ring-BEC experiments in the relevant parameter regime support this assumption [2,4,5].

The resulting condensate density ($|\psi(\phi)|^2$) obtained from the Eqs. (1) and (2), modulated by the presence of the condensate side modes created by the optical lattice, is shown in Fig. 2(a). The OAM content of the modulated condensate density ($|\tilde{\psi}(l)|^2$), where $\tilde{\psi}(l)$ is the Fourier transformation of the condensate wave function $\psi(\phi)$, is shown in Fig. 2(b), which displays the first-order peaks, resulting from matter-wave Bragg diffraction, at $L_p \pm 2\ell$. The figure, which accounts for the full Gross-Pitaevskii condensate dynamics, implies that only three OAM modes are dominant and therefore provides justification for the few-mode model proposed earlier [48].

In Fig. 3(a), we show the phase quadrature of the resulting cavity transmission spectrum [48],

$$S(\omega) = |{\rm Im}[\alpha_{\rm out}(\omega)]|^2, \tag{13}$$

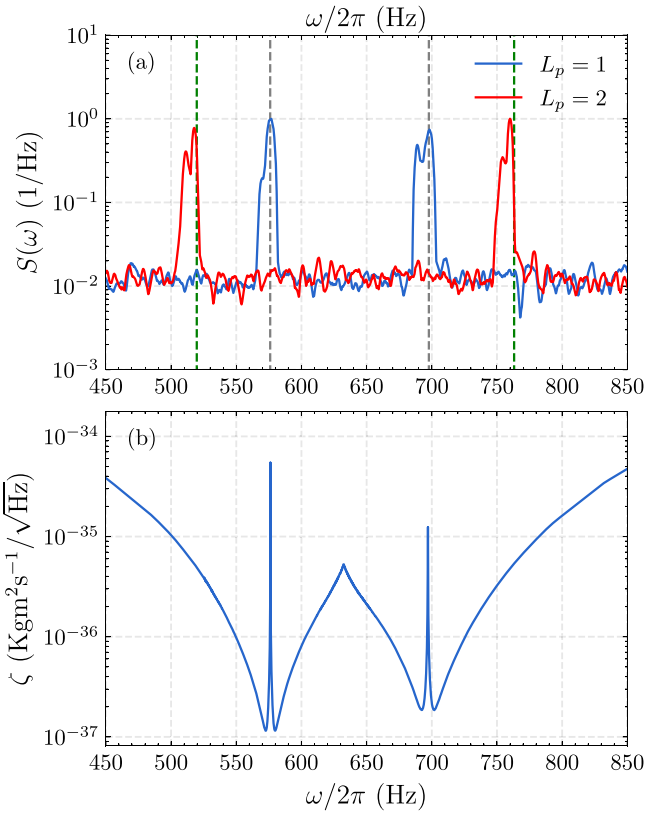

FIG. 3. (a) Power spectra of the output phase quadrature of the cavity field as a function of the system response frequency. The vertical dashed lines (grey and green) correspond to the analytical predictions for the side-mode frequencies of $L_p = 1$ and $L_p = 2$, respectively, including atomic interactions; see Eq. (A13) [48]. (b) Rotation measurement sensitivity ζ [Eq. (14)] as a function of the system response frequency ω. Here $G = 2\pi \times 7.5$ kHz and $|\alpha_s|^2 = 0.096$, which corresponds to $P_{\rm in} = 0.2$ pW. Other parameters are the same as in Fig. 2.

where $\alpha_{\rm out}$ is the output field, transmitted from the cavity, and it is related to the input field into the cavity through the input-output relation $\alpha_{\rm out} = -\alpha_{\rm in} + \sqrt{\gamma_0}\alpha$ [49]. The vertical dashed lines for $L_p = 1$ correspond to the sidemode frequencies $\omega'_{c,d}$ from Eq. (A13) [48,76]. The agreement between the vertical lines and the peak locations shows that the Gross-Pitaevskii simulation retains the results predicted by the analytical theory presented earlier. It also shows that our classical treatment of α, the optical field, reproduces the results of Ref. [48], which treated the optical field quantum mechanically. It can also be seen that the peaks for $L_p = 2$ are spectrally distinct from those for $L_p = 1$. Thus, our method can reliably distinguish between neighboring values of the condensate winding number L_p. We have analyzed the effect of high cavity power drive $P_{\rm in}$ on the power spectra of the output phase of the cavity and find that increasing the $P_{\rm in}$ leads to the deviation of the different peaks of $S(\omega)$ from the analytical results as well as generation of the other OAM modes at higher frequencies as shown in Fig. 10.

We quantify the performance of our scheme by using the sensitivity of the rotation measurement,

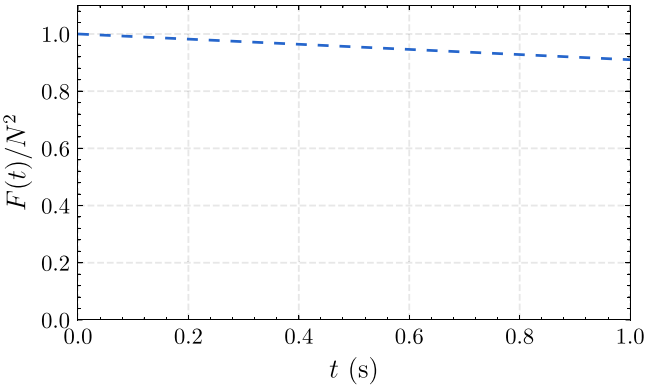

FIG. 4. Variation of the fidelity [Eq. (16)] of the ring condensate density for a persistent current with time. The dashes correspond to the fidelity measured for the wave functions having the same phase profile over time. The set of parameters used are the same as mentioned in Fig. 2.

defined as

$$\zeta = \frac{S(\omega)}{\partial S(\omega)/\partial \Lambda} \times \sqrt{t_{\rm meas}}, \tag{14}$$

where $t_{\rm meas}^{-1} = 8(\alpha_s G)^2/\gamma_0$ is the optomechanical measurement rate in the bad cavity limit, $G = U_0\sqrt{N}/2\sqrt{2}$, α_s is the steady state of the cavity field. Here Λ is the angular momentum of the condensate, defined as [48]

$$\Lambda = \hbar L_p. \tag{15}$$

The sensitivity of Eq. (14), obtained from a fit to the spectrum [Eq. (13)], is displayed in Fig. 3(b), and matches the result from [48] quite well.

To quantify to what extent the measurement backaction affects the condensate, we display the fidelity $F(t)$, i.e., the position-averaged autocorrelation function of the condensate density

$$F(t) = \int_0^{2\pi} |\psi^*(\phi, t)\psi(\phi, 0)|^2 d\phi \tag{16}$$

as a function of the unscaled time t in Fig. 4. As can be seen, the density fidelity stays close to unity for small times. For macroscopic times, it decays mainly due to the damping (Γ) and noise (ξ) of the persistent current. This indicates that the measurement backaction on the condensate is small. Certainly, unlike existing techniques, the measurement does not completely destroy the condensate [1,5].

Before concluding this section, we note that the fidelity can be measured experimentally by absorption imaging, which would destroy the condensate [1,4,16]; our technique of minimally destructive measurement thus applies only to the condensate winding number and not to the fidelity.

2. *Two-state superposition*

In this section, we investigate the dynamics of the condensate prepared in a superposition state of two different winding numbers, i.e., $L_{p1} \neq L_{p2}$, with $L_{p2} > L_{p1}$ without loss of generality. These states could be of interest in the context of quantum information processing, matter-wave interferometry,

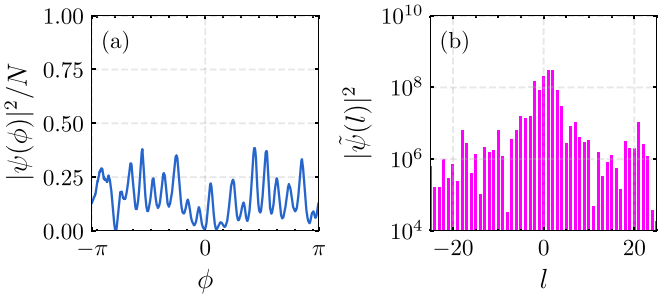

FIG. 5. (a) Angular profile of the condensate density per particle for a persistent current superposition [Eq. (17)] with $L_{p1} = 1$, $L_{p2} = 3$. (b) OAM state content of the condensate. Here $P_{\rm in} = 0.7$ pW and the other parameters are the same as in Fig. 2.

as well as studies of mesoscopic quantum mechanics [77,78]. We restrict our discussion to low values of (L_{p1}, L_{p2}) as superpositions of matter wave vortex states in BECs have so far been produced with winding numbers of magnitude unity [78–80].

We start with the initial state:

$$\psi(\phi) = \sqrt{\frac{N}{4\pi}}(e^{iL_{p1}\phi} + e^{iL_{p2}\phi}). \tag{17}$$

Figures 5(a) and 5(b) show the condensate density and OAM distribution of the condensate wave function resulting from the superposition of two persistent currents with winding numbers $L_{p1} = 1$ and $L_{p2} = 3$ with $P_{in} = 0.7$ pW. The larger modulation in the condensate density and increased complexity in the OAM content of the state (compared to the case of the rotational eigenstate above, see Fig. 2) is due to the complicated interference emerging from the superposition.

All the obtained peaks in the resulting cavity transmission spectrum are presented in Figs. 6(a) and 6(b) for superposition states with winding numbers $L_{p1} = 1, L_{p2} = 3$ and $L_{p1} = 2, L_{p2} = 3$, respectively. In these simulations, the peaks were identified in the following manner. The dominant peak(s) were used to identify the smaller winding number L_{p1} (this effect can be traced to the dependence of the optomechanical couplings on the sidemode frequencies [48]). For example, the two dominant peaks in Fig. 6(a) were found to correspond to the analytical predictions of Eq. (A13) [48,76] for the side modes at $L_{p1} \pm 2l$. In Fig. 6(b), the dominant peak near 760 Hz was found to correspond to $L_{p1} + 2l$. These identifications allowed for all other peaks related to L_{p1} to be assigned in Figs. 6(a) and 6(b), respectively. On the other hand, the outermost peaks in both spectra were found to be due to the larger of the two winding numbers when the numerical peak positions were compared with the analytical predictions of Eq. (A13) [48,76]. For example, in Figs. 6(a) and 6(b), the outermost peaks correspond to the winding numbers $L_{p2} \pm 2l$. To show the absence of peaks beyond these positions in the spectrum, purple vertical dashed lines have been drawn to indicate the analytical predictions for the peaks corresponding to $L_{p2} \pm 2l + 1$. In both cases, we notice some mismatch between the analytical predictions, given by the vertical dashed lines and the positions of the simulated peaks, but they are close enough to make the assignments unambiguous. For general values of L_{p1} and L_{p2}, the identification strategy will

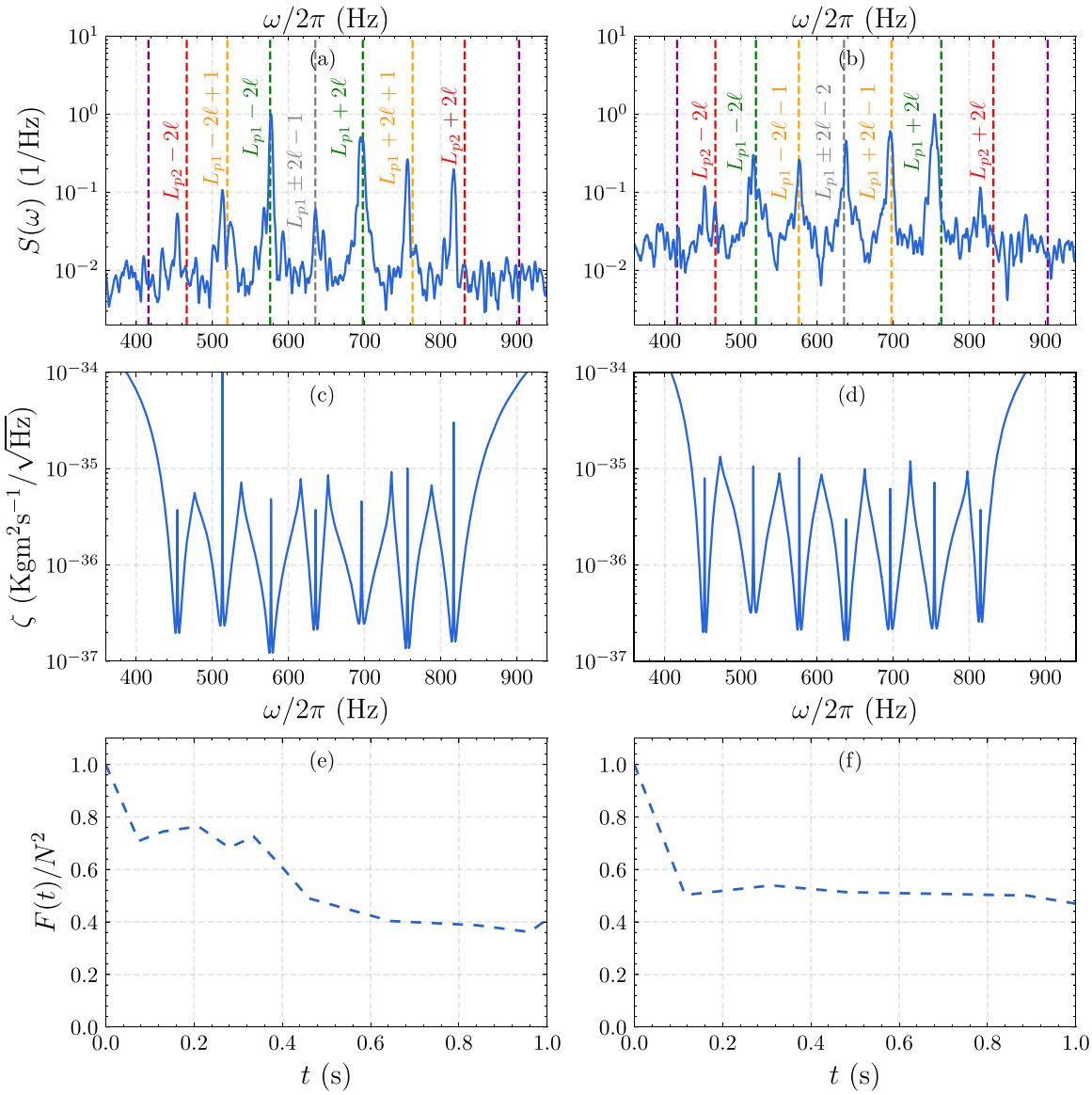

FIG. 6. Persistent current superposition of two combinations of winding numbers: Left column for $L_{p1} = 1$ and $L_{p2} = 3$ and right column for $L_{p1} = 2$ and $L_{p2} = 3$. (a) and (b) represent the cavity output spectrum, (c) and (d) show the rotation measurement sensitivities, and (e) and (f) are the temporal evolutions of the fidelity for $L_{p1} = 1$, $L_{p2} = 3$ and $L_{p1} = 2$, $L_{p2} = 3$, respectively. Vertical dashed lines represent the analytical prediction corresponding to the $L_{p1} \pm 2l$, $L_{p2} \pm 2l$ modes and their combinations (Eq. (A13) [48,76]. Here $G = 2\pi \times 7.5$ kHz, $|\alpha_s|^2 = 0.33$, and the optomechanical measurement time (t_{meas}) is 2.1 ms. All other parameters used are the same as in Fig. 5.

likely involve comparing the experimental data with templates from the numerical simulation.

The sensitivities of the rotation measurement for the above-discussed two cases are shown in Figs. 6(c) and 6(d), respectively. We achieve improved sensitivity in the proximity of each of the side modes resulting from the superposition of the L_{p1} and L_{p2} states.

Figures 6(e) and 6(f) illustrate the fidelity over time for the two above-mentioned cases. The degradation of fidelity is notably faster in this scenario compared to the single-state persistent current case (Fig. 4). This dissimilarity arises from the presence of multiple states due to the superposition and their resulting interference pattern, which is not robust against external noise and phase fluctuations. The dashed curve provides a clear visual representation of the highest fidelity levels attained throughout the temporal evolution of the system, which is near $\sim 0.5 - 0.75$ in the best case. Although such fidelities may seem low for a technique that aims at minimal destruction, they compared very favorably to currently available techniques, all of which give a fidelity of zero, since they are totally destructive of the condensate [1,4,5].

B. Bright soliton

This section presents the dynamics accompanying the detection of a bright soliton in the ring BEC. Such solitons can be sustained by condensates in which the atoms weakly attract

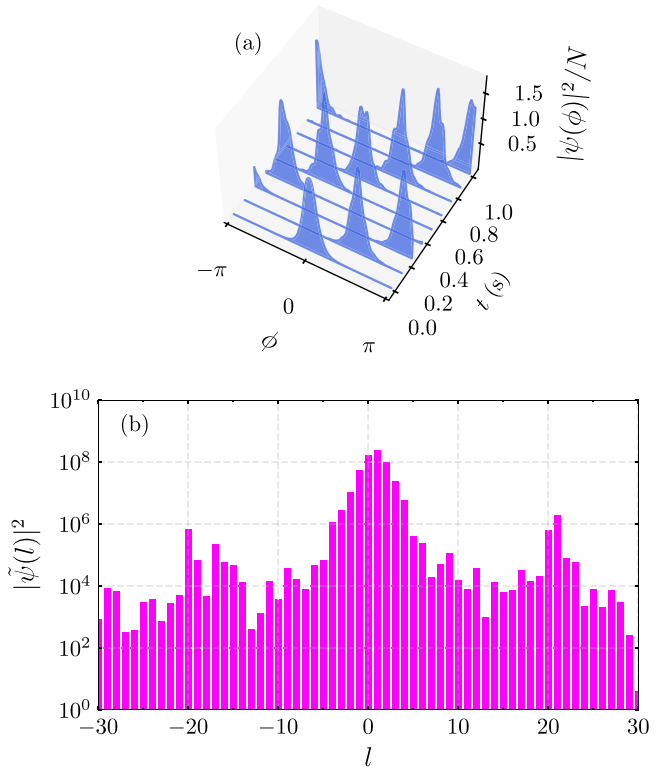

FIG. 7. (a) Temporal evolution of the soliton density profile (b) OAM content of the soliton. Here $N = 6000$, $a_s = -27.6a_0$, where a_0 is the Bohr radius, $m = 7.01$ amu, $L_p = 1$, and $P_{\text{in}} = 0.4$ pW, and all other parameters are same as in Fig. 2.

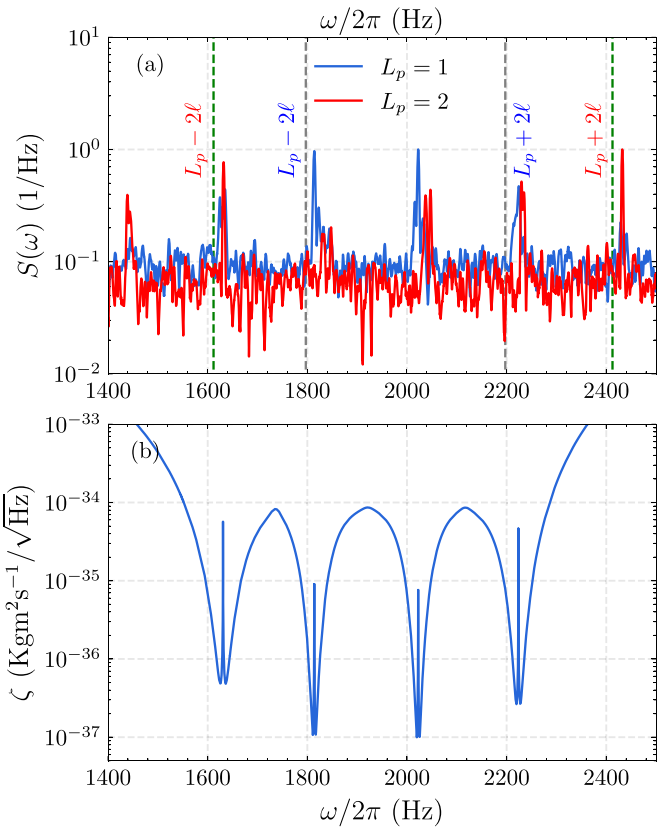

FIG. 8. (a) Power spectrum of the output phase quadrature of the cavity field as a function of the system response frequency for a soliton. The vertical dashed lines (grey and green) correspond to the analytical predictions for the side modes ($L_p \pm 2\ell$) of $L_p = 1$ and $L_p = 2$, respectively, see Eq. (A13) [48,76]. Only the corresponding peaks have been labeled. (b) Variation of rotation measurement sensitivity ζ with the system response frequency ω for $L_p = 1$. Here $G = 2\pi \times 5.8$ kHz and $|\alpha_s|^2 = 0.192$, which corresponds to $P_{in} = 0.4$ pW. The other set of parameters used here are the same as in Fig. 7.

each other [81–91] and have been considered for interferometry on a ring [62].

In our simulations, we imprint a density and phase modulation on a uniform condensate of ^{7}Li atoms [88] and this leads to a bright soliton rotating on the ring and carrying a winding number L_p (e.g., see Eq. (43) of Ref. [76]). For this situation, we consider the initial state as

$$\psi(\phi) = \sqrt{\frac{N}{\sqrt{\pi}}} e^{-\phi^2/2} e^{iL_p\phi}. \tag{18}$$

For $L_p = 1$, the temporal evolution of the soliton density profile is shown in Fig. 7(a). As can be seen, the spatial profile of the soliton stays close to its initial shape as it moves in the ring and is probed by the weak optical lattice. The OAM distribution of the soliton, when it has interacted with the optical lattice, is shown in Fig. 7(b).

The resulting cavity transmission spectrum used to detect the winding number of the soliton is shown in Fig. 8(a). As can be seen, the $L_p = 1$ and $L_p = 2$ peaks are resolvable, indicating that our method can distinguish between neighboring winding numbers for the soliton. Remarkably, the predictions for the spectral locations of the side-mode peaks from the analytical treatment of the persistent current case, see Eq. (A13) [48,76], are quite close to the numerical results for the full Gross-Pitaevskii treatment of the soliton [48]. This can be seen from the comparison of the numerically obtained side mode peak locations and the vertical dashed lines in Fig. 8(a).

The corresponding measurement sensitivity is shown in Fig. 8(b). As can be seen, the benefits of high measurement sensitivities in our optomechanical scheme carry over from the persistent current case (where it was three orders of magnitude better than demonstrated previously [48]) to the case of the bright soliton. The fidelity of the density profile is shown in Fig. 9 and remains close to unity for macroscopic times. The decay in fidelity is largely due to the dissipation (Γ) and noise (ξ) in the system and not so much due to measurement backaction. Hence, our scheme represents a minimally destructive measurement of the motion of a bright soliton in a ring BEC.

We note that, in contrast to the case of the fidelity of the superposition of two persistent currents, which decays more rapidly [Figs. 6(e) and 6(f)], the fidelity of a soliton, which is a superposition of many persistent currents, decays much more slowly (Fig. 9). This is because, unlike the case of the two-current superposition, which involves repulsive atomic interactions, the soliton involves attractive atomic interactions. This attraction maintains the form of the soliton and, hence, the fidelity for longer times. We have found in

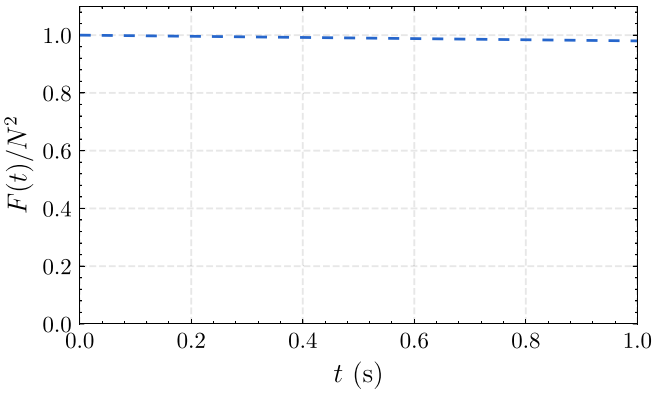

FIG. 9. Fidelity [Eq. (16)] of the soliton density profile versus time. The dashes correspond to the fidelity measured for the wave functions having the same phase profile over time. The set of parameters used is the same as in Fig. 7.

our simulations that the soliton shape is less well preserved if the strength of the atomic interactions is lowered. We also note that our technique is not capable of identifying whether the excitation is a soliton or not. Thus, we have assumed, as in experiments, that this is known beforehand [61].

IV. SUMMARY AND CONCLUSIONS

Using a stochastic mean-field Gross-Pitaevskii formalism for modeling atoms in a BEC in a ring trap, and a classical approximation for the optical mode, we have demonstrated that cavity optomechanics can make real-time, *in situ*, and minimally destructive measurements of both persistent currents as well as bright solitons. In support of our conclusions, we have presented numerical simulations of cavity transmission spectra, measurement sensitivities as a function of the system response frequency, and the fidelities of condensate density profiles.

Our numerical simulations have verified and extended the analytical model proposed by us earlier [48]. Remarkably, the previously analytically found locations of the peaks in the cavity transmission crucial for determining condensate rotation agree well with the numerical results for both persistent current states as well as solitons.

We expect our findings to be of interest to studies of superfluid hydrodynamics, atomtronics, and soliton interferometry. The technique we have presented could be extended to other systems such as polariton ring condensates [92]. One of the future directions of the work will include the systematic investigation of the effect of optical power and relative phase on the interference.

ACKNOWLEDGMENTS

We thank the International Centre for Theoretical Sciences (ICTS), Bengaluru, where this work was initiated, for hosting us during the discussion meeting on Structured Light and Spin-Orbit Photonics (Code No. ICTS/slsop2022/11). M.B. thanks the Air Force Office of Scientific Research (FA9550-23-1-0259) for support. R.K. acknowledges support from JSPS KAKENHI Grant No. JP21K03421. P.K. acknowledges financial support from the Max Planck Society. We also gratefully acknowledge our supercomputing facility Param-Ishan (IITG), where all the simulation runs were performed.

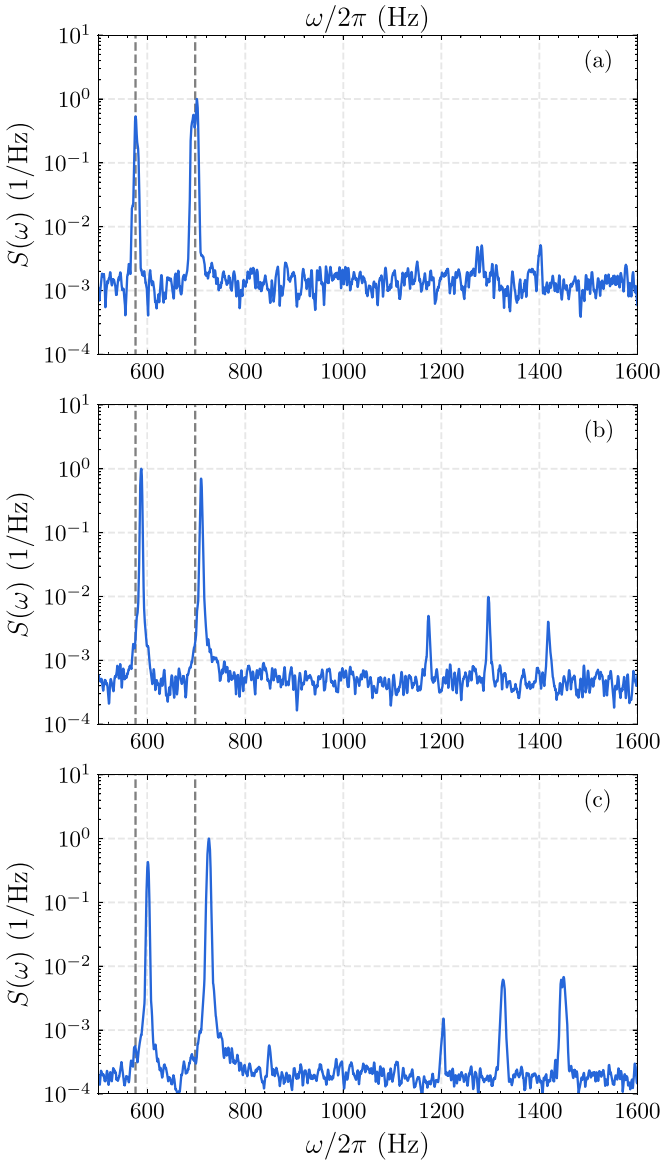

FIG. 10. Power spectrum of the output phase quadrature of the cavity field as a function of the system response frequency for different input powers: (a) $P_{\text{in}} = 0.5$ pW, (b) $P_{\text{in}} = 1$ pW, and (c) $P_{\text{in}} = 2$ pW. Vertical dashed lines indicate the analytical predictions of Eq. (A13) [48,76]. All other parameters used are the same as in Fig. 2.

APPENDIX A: SUMMARY OF THE THEORETICAL MODEL

In this Appendix, we summarize the mathematical model of our system, which was presented in an earlier publication [48], to make the present work self-contained.

1. Light-matter interaction

As described in the main text, we consider a ring BEC confined inside an optical resonator driven by a superposition of Laguerre-Gaussian beams carrying OAM $\pm\ell\hbar$, as shown in Fig. 1. Using a two-level description of the condensate atoms and working in the limit of large atom-photon detuning, the dispersive light-matter interaction is governed by [48]

$$H_{a-f} \approx \frac{\hbar \mathcal{D}_{eg}^2 \mathcal{E}_0^2 |u_{+\ell 0}(\mathbf{r}) + u_{-\ell 0}(\mathbf{r})|^2}{\Delta_a} a^\dagger a, \tag{A1}$$

where $\mathcal{D}_{eg}$ is the matrix element of the atomic transition dipole moment operator, Δ_a is the detuning of the drive laser from atomic frequency, and $\mathcal{E}_0$ is the single photon electric field. The field bosonic operators obey the commutation relation $[a, a^\dagger] = 1$. Here, $u_{\pm\ell 0}(\mathbf{r})$ are the mode functions corresponding to the optical beams of OAM $\pm\ell\hbar$. To a good approximation, the magnitude of these mode functions near $z = 0$ can be written as $|u_{+\ell 0}(\mathbf{r}) + u_{-\ell 0}(\mathbf{r})|^2 \approx \cos(\ell\phi)$. Using this information, we write the following coupling Hamiltonian governing the interaction of the condensate with the cavity field:

$$H_{a-f} \approx \frac{\hbar g_a^2 \cos^2(\ell\phi)}{\Delta_a} a^\dagger a = \hbar U_0 \cos^2(\ell\phi) a^\dagger a. \tag{A2}$$

Taking into account the above light-matter interaction, the atomic many-body Hamiltonian in the frame rotating at the drive laser frequency and describing the azimuthal motion of BEC is written as

$$H = \int_0^{2\pi} d\phi \Psi^\dagger(\phi) \left[\mathcal{H}^{(1)} + \frac{g}{2} \Psi^\dagger(\phi)\Psi(\phi) \right] \Psi(\phi) + \mathcal{H}_c, \tag{A3}$$

where g denotes the strength of two-body atomic interaction. The single-atom Hamiltonian,

$$\mathcal{H}^{(1)} = -\frac{d^2}{d\phi^2} + H_{a-f}, \tag{A4}$$

includes the contribution from the rotational kinetic energy of the atoms (first term) and the dispersive interaction between the atoms and the drive (second term). The last term in Eq. (A3),

$$\mathcal{H}_c = -\hbar\Delta_o a^\dagger a + i\hbar\eta(a^\dagger - a), \tag{A5}$$

contains contributions from the energy of the cavity field and the laser drive. Using Eq. (A3), the classical mean-field equations can be derived, which, after including fluctuations, are expressed in Eqs. (1) and (2). This derivation is quite involved; the general technique is provided in Refs. [67,68], and equations analogous to Eqs. (1) and (2) are typically presented as the starting point of BEC-cavity systems analysis [93,94].

We note that the stochastic term $\xi(\phi, \tau)$ in Eq. (1) is analogous to the Brownian noise and arises from the randomness of the incoherent collisions in the system [68]. Through the fluctuation-dissipation theorem, this also sets the damping of the persistent current. On the other hand, the physical origin of the noise term $\alpha_{\text{in}}(\tau)$ in Eq. (2) is due to the leakage of photons and the entry of vacuum fluctuations through the mirrors, which provide dissipation and noise to the cavity [49].

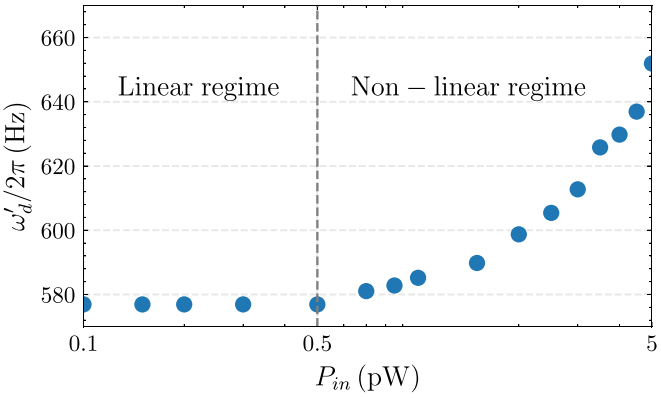

FIG. 11. Location of the peak in the output spectrum ($\omega_d'/2\pi$) [Eq. (A13)] [48,76] versus input optical power (P_{in}). All other parameters are the same as in Fig. 2. For $P_{\text{in}} \lesssim 0.5$ pW, the location of the $\omega_d'/2\pi$ peak remains constant, implying the presence of linear response; while for higher power ($P_{\text{in}} \gtrsim 0.5$ pW), the $\omega_d'/2\pi$ peak begins to deviate from the linear regime, indicating the nonlinear response.

2. Other relevant equations

The detection of ring BEC rotation in our model is based on the cavity transmission signal. To make our model self-contained, here we discuss the relevant physical processes governing the transmission. For this, we consider a weak dipole potential and take into account only the first-order Bragg diffraction of atoms from their rotational state of winding number L_p to $L_p \pm 2\ell$. This two-side-mode description is equivalent to an optomechanical interaction coupling two mechanical oscillators with a single cavity mode. The relevant quantum Langevin equations of motion for such a model are written in terms of dimensionless position quadratures X_j, (where j is defined below) in the following form [48]:

$$\ddot{X}_j + \gamma_m \dot{X}_j + \Omega_j^2 X_j \pm \mathcal{A} X_k = -\tilde{\omega}_j G a^\dagger a + \omega_j \epsilon_j, \tag{A6}$$

$$\dot{a} + \left[\frac{\gamma_o}{2} - i\left(\tilde{\Delta} - G \sum_{j=c,d} X_j \right) \right] a = \eta + \sqrt{\gamma_o} a_{\text{in}}, \tag{A7}$$

where $j, k = c, d$ $(j \neq k)$, $\tilde{\Delta} = \Delta_c - (U_0 N)/2$ and $G = U_o\sqrt{N/8}$. Other quantities are defined as

$$\Omega_j^2 = (\omega_j + 2\omega_{\text{coll}})^2 - \omega_{\text{coll}}^2, \tag{A8}$$

$$\tilde{\omega}_j = \omega_j + \omega_{\text{coll}}, \tag{A9}$$

$$\mathcal{A} = \omega_{\text{coll}}(\omega_c - \omega_d), \tag{A10}$$

where $\omega_{\text{coll}} = 2\tilde{g}N$, $\tilde{g} = g/(4\pi\hbar)$, and side-mode frequencies in the absence of atomic interactions are expressed in terms of ω_β as

$$\omega_c = \omega_\beta (L_p + 2\ell)^2, \tag{A11}$$

$$\omega_d = \omega_\beta (L_p - 2\ell)^2. \tag{A12}$$

While $\omega_{c,d}$ ($\Omega_{c,d}$) are the side-mode frequencies in the absence (presence) of collisions obtained by the linearization procedure which considers two modes of the condensate, a full

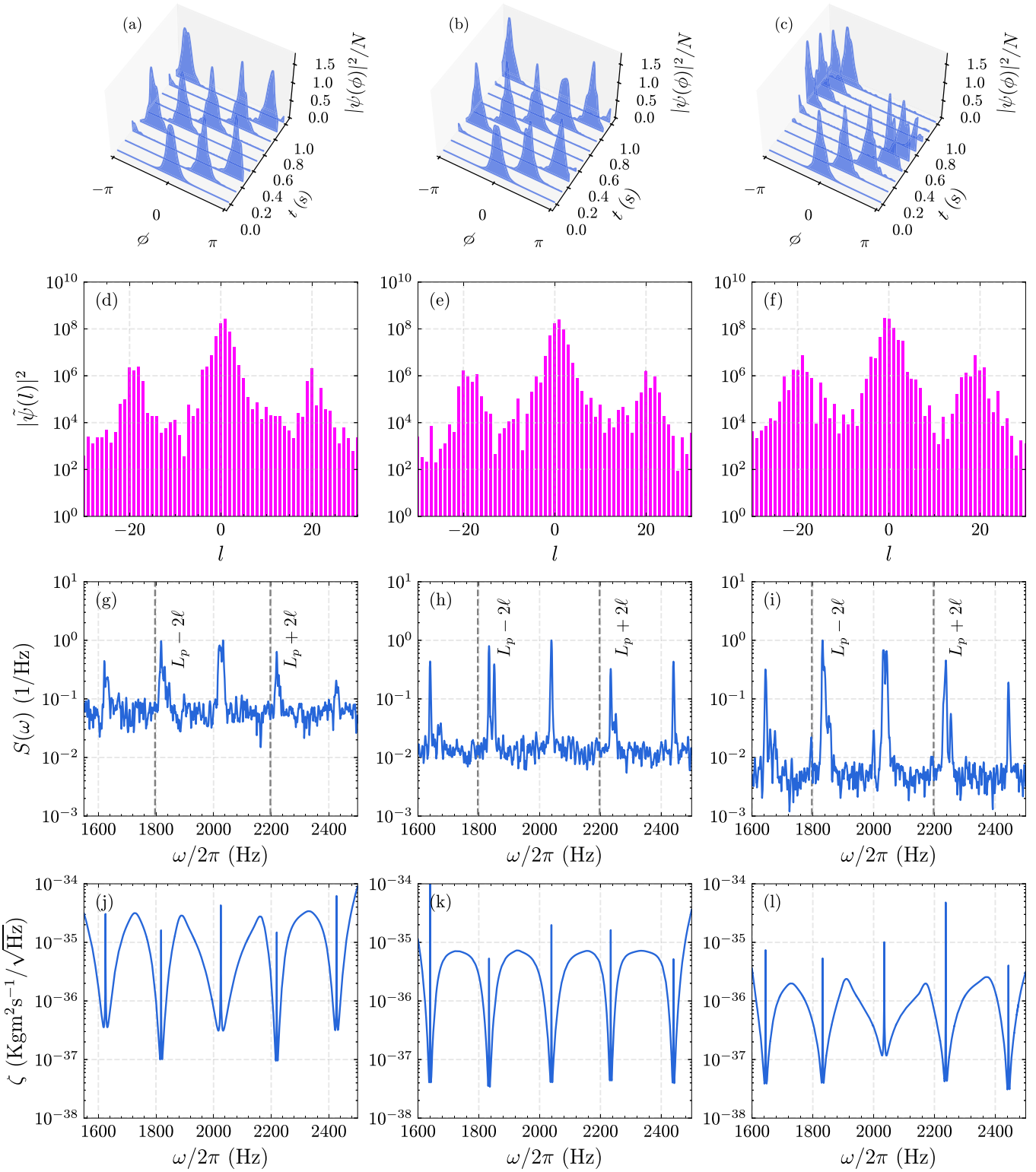

FIG. 12. (a)–(c) Temporal evolution of the moving soliton density profile. (d)–(f) OAM states of the condensate occupied by the soliton. (g)–(i) Power spectrum of the phase quadrature of the cavity field versus system response frequency. Vertical dashed lines indicate the analytical predictions of the side modes for $L_p \pm 2\ell$, Eq. (A13) [48,76]. (j)–(l) Soliton rotation measurement sensitivity as a function of system response frequency for $P_{\text{in}} = 0.7$ pW, 1 pW, and 2 pW, respectively. Here $G = 2\pi \times 5.8$ kHz and $|\alpha_s|^2 = 0.33, 0.48, 0.96$, respectively, for the above input power values. The remaining parameters are the same as in Fig. 7.

Bogoliubov analysis yields the frequencies [48,76]

$$\omega'_{c,d} = [\omega_{c,d}(\omega_{c,d} + 4\tilde{g}N)]^{1/2}, \tag{A13}$$

which are actually the appropriate quantities to be compared to the numerical simulations. Further, in Eqs. (A6) and (A7), γ_m and γ_o represent the damping of the side modes and cavity, respectively. The quantities ϵ_j and $a_{\rm in}$ are delta-correlated mechanical side-mode and optical fluctuations of zero mean.

In the analytical treatment, to model the detection of ring BEC rotation, we write the equations for fluctuations by linearizing Eqs. (A6) and (A7) around the steady-state values of the system variables. Then we model homodyne measurement of the cavity output field $a_{\rm out}(t) = -a_{\rm in}(t) + \sqrt{\gamma_o}a$ to obtain the noise spectrum of the phase quadrature.

APPENDIX B: RESULTS FOR HIGH INPUT POWER

In this Appendix, we present the effect of increasing the cavity drive power $P_{\rm in}$ and thus making a stronger measurement of the persistent current and bright soliton rotation. For simplicity, we omit the results for persistent current superpositions. Generally, we find that increasing the power leads to shifts in the positions of the desired peaks (which yield the condensate winding number) and to the appearance of additional peaks that are irrelevant to the measurement of the condensate winding number. These observations imply the conclusion that, since measurement is our main aim, the high-power, nonlinear regime must be avoided.

1. Persistent currents: Rotational eigenstate

In Fig. 10, we show the power spectra of the output phase quadrature of the cavity field in the frequency domain for three different input powers, namely, $P_{\rm in} = 0.5$ pW, 1 pW, and 2 pW for the persistent current rotational eigenstate [Eq. (12)].

We find that increasing the power [from Fig. 10(a) to Fig. 10(c)] leads to the nonlinear response of the system since the optical lattice becomes deeper and can no longer be treated perturbatively via linearization as in previous work [48]. This results in the undesirable deviation of the peak locations from the analytically predicted values (which interferes with the measurement of the condensate winding number) and the emergence of higher frequencies in the cavity output spectrum (which are irrelevant to the measurement in addition to being complicated to characterize).

To characterize the parameter regime where this deviation occurs, we have depicted the shift in peak location of $\omega'_d/2\pi$ [Eq. (A13)] with respect to the input optical power in Fig. 11. As can be seen from the figure, the BEC-cavity system operates linearly within a regime of $P_{\rm in} < 0.5$ pW. Beyond this threshold, an increase in the input power propels the system into the nonlinear regime.

2. Soliton

Density profiles of the ring condensate with the soliton have been shown for various $P_{\rm in}$ in Figs. 12(a)–12(c). We can see that at low powers, $P_{\rm in}$ the density profile is only slightly modulated, while it is quite heavily modulated at high $P_{\rm in}$. Thus, as expected, the measurement backaction increases with cavity power. However, in the entire regime of the powers presented, the soliton does not break up as a result of interaction with the probe lattice, and thus the measurement is not fully destructive.

The OAM content of the soliton for the corresponding powers has been shown in Figs. 12(d)–12(f). The cavity output spectra are displayed in Figs. 12(g)–12(i), with peaks labeled by the winding number L_p. For clarity, only the vertical dashed lines corresponding to the analytical $L_p \pm 2\ell$ side-mode frequencies Eq. (A13) [48,76] have been shown. As can be seen, the use of higher optical powers results in additional peaks, more noise, and increasing deviation from the analytical peak-location values due to the nonlinear response. Finally, the sensitivities are shown in Figs. 12(j)–12(l), revealing comparable patterns to those observed in the low-power version (Fig. 8).

[1] C. Ryu, M. F. Andersen, P. Cladé, V. Natarajan, K. Helmerson, and W. D. Phillips, Observation of persistent flow of a Bose-Einstein condensate in a toroidal trap, Phys. Rev. Lett. **99**, 260401 (2007).

[2] Y. Guo, R. Dubessy, M. d. G. de Herve, A. Kumar, T. Badr, A. Perrin, L. Longchambon, and H. Perrin, Supersonic rotation of a superfluid: A long-lived dynamical ring, Phys. Rev. Lett. **124**, 025301 (2020).

[3] Y. Guo, E. M. Gutierrez, D. Rey, T. Badr, T. Perrin, L. Longchambon, V. S. Bagnato, H. Perrin, and R. Dubessy, Expansion of a quantum gas in a shell trap, New J. Phys. **24**, 093040 (2022).

[4] S. Moulder, S. Beattie, R. P. Smith, N. Tammuz, and Z. Hadzibabic, Quantized supercurrent decay in an annular Bose-Einstein condensate, Phys. Rev. A **86**, 013629 (2012).

[5] K. C. Wright, R. B. Blakestad, C. J. Lobb, W. D. Phillips, and G. K. Campbell, Driving phase slips in a superfluid atom circuit with a rotating weak link, Phys. Rev. Lett. **110**, 025302 (2013).

[6] K. Snizhko, K. Isaieva, Y. Kuriatnikov, Y. Bidasyuk, S. Vilchinskii, and A. Yakimenko, Stochastic phase slips in toroidal Bose-Einstein condensates, Phys. Rev. A **94**, 063642 (2016).

[7] K. C. Wright, R. B. Blakestad, C. J. Lobb, W. D. Phillips, and G. K. Campbell, Threshold for creating excitations in a stirred superfluid ring, Phys. Rev. A **88**, 063633 (2013).

[8] S. Beattie, S. Moulder, R. J. Fletcher, and Z. Hadzibabic, Persistent currents in spinor condensates, Phys. Rev. Lett. **110**, 025301 (2013).

[9] A. Gallemí, A. M. Mateo, R. Mayol, and M. Guilleumas, Coherent quantum phase slip in two-component bosonic atomtronic circuits, New J. Phys. **18**, 015003 (2015).

[10] S. Eckel, J. Lee, F. Jendrzejewski, N. Murray, C. W. Clark, C. J. Lobb, W. D. Phillips, M. Edwards, and G. K. Campbell, Hysteresis in a quantized superfluid 'atomtronic' circuit, Nature (London) **506**, 200 (2014).

[11] J. Hou, X.-W. Luo, K. Sun, and C. Zhang, Adiabatically tuning quantized supercurrents in an annular Bose-Einstein condensate, Phys. Rev. A **96**, 011603(R) (2017).

[12] Y. H. Wang, A. Kumar, F. Jendrzejewski, R. M. Wilson, M. Edwards, S. Eckel, G. K. Campbell, and C. W. Clark, Resonant wavepackets and shock waves in an atomtronic SQUID, New J. Phys. **17**, 125012 (2015).

[13] S. Gupta, K. W. Murch, K. L. Moore, T. P. Purdy, and D. M. Stamper-Kurn, Bose-Einstein condensation in a circular waveguide, Phys. Rev. Lett. **95**, 143201 (2005).

[14] G. E. Marti, R. Olf, and D. M. Stamper-Kurn, Collective excitation interferometry with a toroidal Bose-Einstein condensate, Phys. Rev. A **91**, 013602 (2015).

[15] A. Ramanathan, K. C. Wright, S. R. Muniz, M. Zelan, W. T. Hill, C. J. Lobb, K. Helmerson, W. D. Phillips, and G. K. Campbell, Superflow in a toroidal Bose-Einstein condensate: An atom circuit with a tunable weak link, Phys. Rev. Lett. **106**, 130401 (2011).

[16] C. Ryu, P. W. Blackburn, A. A. Blinova, and M. G. Boshier, Experimental realization of Josephson junctions for an atom SQUID, Phys. Rev. Lett. **111**, 205301 (2013).

[17] S. Pandey, H. Mas, G. Vasilakis, and W. von Klitzing, Atomtronic matter-wave lensing, Phys. Rev. Lett. **126**, 170402 (2021).

[18] L. Amico, D. Anderson, M. Boshier, J.-P. Brantut, L.-C. Kwek, A. Minguzzi, and W. von Klitzing, Colloquium: Atomtronic circuits: From many-body physics to quantum technologies, Rev. Mod. Phys. **94**, 041001 (2022).

[19] J. J. Cooper, D. W. Hallwood, and J. A. Dunningham, Entanglement-enhanced atomic gyroscope, Phys. Rev. A **81**, 043624 (2010).

[20] G. Pelegrí, J. Mompart, and V. Ahufinger, Quantum sensing using imbalanced counter-rotating Bose–Einstein condensate modes, New J. Phys. **20**, 103001 (2018).

[21] R. Kanamoto, L. D. Carr, and M. Ueda, Topological winding and unwinding in metastable Bose-Einstein condensates, Phys. Rev. Lett. **100**, 060401 (2008).

[22] A. Das, J. Sabbatini, and W. H. Zurek, Winding up superfluid in a torus via Bose Einstein condensation, Sci. Rep. **2**, 352 (2012).

[23] L. Corman, L. Chomaz, T. Bienaimé, R. Desbuquois, C. Weitenberg, S. Nascimbène, J. Dalibard, and J. Beugnon, Quench-induced supercurrents in an annular Bose gas, Phys. Rev. Lett. **113**, 135302 (2014).

[24] S. Eckel, A. Kumar, T. Jacobson, I. B. Spielman, and G. K. Campbell, A rapidly expanding Bose-Einstein condensate: An expanding universe in the Lab, Phys. Rev. X **8**, 021021 (2018).

[25] P. Öhberg and E. M. Wright, Quantum time crystals and interacting gauge theories in atomic Bose-Einstein condensates, Phys. Rev. Lett. **123**, 250402 (2019).

[26] R. Kanamoto, H. Saito, and M. Ueda, Quantum phase transition in one-dimensional Bose-Einstein condensates with attractive interactions, Phys. Rev. A **67**, 013608 (2003).

[27] S. Baharian and G. Baym, Bose-Einstein condensates in toroidal traps: Instabilities, swallow-tail loops, and self-trapping, Phys. Rev. A **87**, 013619 (2013).

[28] I. Yatsuta, B. Malomed, and A. Yakimenko, Acoustic analog of Hawking radiation in quantized circular superflows of Bose-Einstein condensates, Phys. Rev. Res. **2**, 043065 (2020).

[29] M. Todorić, B. Klajn, D. Jukić, and H. Buljan, Berry phase for a Bose gas on a one-dimensional ring, Phys. Rev. A **102**, 013322 (2020).

[30] D. Aghamalyan, M. Cominotti, M. Rizzi, D. Rossini, F. Hekking, A. Minguzzi, L.-C. Kwek, and L. Amico, Coherent superposition of current flows in an atomtronic quantum interference device, New J. Phys. **17**, 045023 (2015).

[31] F. Piazza, L. A. Collins, and A. Smerzi, Critical velocity for a toroidal Bose–Einstein condensate flowing through a barrier, J. Phys. B: At. Mol. Opt. Phys. **46**, 095302 (2013).

[32] E. Arabahmadi, D. Schumayer, M. Edwards, B. Eller, and D. A. W. Hutchinson, Thermal stability of a quantum rotation sensor, Phys. Rev. A **104**, 033323 (2021).

[33] A. C. Mathey, C. W. Clark, and L. Mathey, Decay of a superfluid current of ultracold atoms in a toroidal trap, Phys. Rev. A **90**, 023604 (2014).

[34] M. Kunimi and I. Danshita, Decay mechanisms of superflow of Bose-Einstein condensates in ring traps, Phys. Rev. A **99**, 043613 (2019).

[35] J. Polo, R. Dubessy, P. Pedri, H. Perrin, and A. Minguzzi, Oscillations and decay of superfluid currents in a one-dimensional Bose gas on a ring, Phys. Rev. Lett. **123**, 195301 (2019).

[36] Z. Mehdi, A. S. Bradley, J. H. Hope, and S. S. Szigeti, Superflow decay in a toroidal Bose gas: The effect of quantum and thermal fluctuations, SciPost Phys. **11**, 080 (2021).

[37] M. Modugno, C. Tozzo, and F. Dalfovo, Detecting phonons and persistent currents in toroidal Bose-Einstein condensates by means of pattern formation, Phys. Rev. A **74**, 061601(R) (2006).

[38] H. Huang and K. K. Das, Effects of a rotating periodic lattice on coherent quantum states in a ring topology: The case of positive nonlinearity, Phys. Rev. A **104**, 053320 (2021).

[39] S. Ragole and J. M. Taylor, Interacting atomic interferometry for rotation sensing approaching the Heisenberg limit, Phys. Rev. Lett. **117**, 203002 (2016).

[40] M. Cominotti, D. Rossini, M. Rizzi, F. Hekking, and A. Minguzzi, Optimal persistent currents for interacting bosons on a ring with a gauge field, Phys. Rev. Lett. **113**, 025301 (2014).

[41] F. Kiałka, B. A. Stickler, and K. Hornberger, Orbital angular momentum interference of trapped matter waves, Phys. Rev. Res. **2**, 022030 (2020).

[42] J. Brand, T. J. Haigh, and U. Zülicke, Rotational fluxons of Bose-Einstein condensates in coplanar double-ring traps, Phys. Rev. A **80**, 011602(R) (2009).

[43] A. Oliinyk, A. Yakimenko, and B. Malomed, Tunneling of persistent currents in coupled ring-shaped Bose–Einstein condensates, J. Phys. B: At. Mol. Opt. Phys. **52**, 225301 (2019).

[44] A. Pérez-Obiol, J. Polo, and L. Amico, Coherent phase slips in coupled matter-wave circuits, Phys. Rev. Res. **4**, L022038 (2022).

[45] A. Muñoz Mateo, A. Gallemí, M. Guilleumas, and R. Mayol, Persistent currents supported by solitary waves in toroidal Bose-Einstein condensates, Phys. Rev. A **91**, 063625 (2015).

[46] A. Kumar, N. Anderson, W. D. Phillips, S. Eckel, G. K. Campbell, and S. Stringari, Minimally destructive, Doppler measurement of a quantized flow in a ring-shaped Bose–Einstein condensate, New J. Phys. **18**, 025001 (2016).

[47] S. Safaei, L.-C. Kwek, R. Dumke, and L. Amico, Monitoring currents in cold-atom circuits, Phys. Rev. A **100**, 013621 (2019).

[48] P. Kumar, T. Biswas, K. Feliz, R. Kanamoto, M.-S. Chang, A. K. Jha, and M. Bhattacharya, Cavity optomechanical sensing and manipulation of an atomic persistent current, Phys. Rev. Lett. **127**, 113601 (2021).

[49] M. Aspelmeyer, T. J. Kippenberg, and F. Marquardt, Cavity optomechanics, Rev. Mod. Phys. **86**, 1391 (2014).

[50] B. P. Abbott, R. Abbott, T. D. Abbott, M. R. Abernathy, F. Acernese, K. Ackley, C. Adams, T. Adams, P. Addesso, R. X. Adhikari *et al.* (LIGO Scientific Collaboration and Virgo Collaboration), Observation of gravitational waves from a binary black hole merger, Phys. Rev. Lett. **116**, 061102 (2016).

[51] A. G. Krause, M. Winger, T. D. Blasius, Q. Lin, and O. Painter, A high-resolution microchip optomechanical accelerometer, Nat. Photonics **6**, 768 (2012).

[52] S. Forstner, S. Prams, J. Knittel, E. D. van Ooijen, J. D. Swaim, G. I. Harris, A. Szorkovszky, W. P. Bowen, and H. Rubinsztein-Dunlop, Cavity optomechanical magnetometer, Phys. Rev. Lett. **108**, 120801 (2012).

[53] V. Montenegro, M. G. Genoni, A. Bayat, and M. G. A. Paris, Mechanical oscillator thermometry in the nonlinear optomechanical regime, Phys. Rev. Res. **2**, 043338 (2020).

[54] M. Sansa, M. Defoort, A. Brenac, M. Hermouet, L. Banniard, A. Fafin, M. Gely, C. Masselon, I. Favero, G. Jourdan, and S. Hentz, Optomechanical mass spectrometry, Nat. Commun. **11**, 3781 (2020).

[55] S. Schreppler, N. Spethmann, N. Brahms, T. Botter, M. Barrios, and D. M. Stamper-Kurn, Optically measuring force near the standard quantum limit, Science **344**, 1486 (2014).

[56] F. Fogliano, B. Besga, A. Reigue, L. M. de Lépinay, P. Heringlake, C. Gouriou, E. Eyraud, W. Wernsdorfer, B. Pigeau, and O. Arcizet, Ultrasensitive nano-optomechanical force sensor operated at dilution temperatures, Nat. Commun. **12**, 4124 (2021).

[57] F. Brennecke, S. Ritter, T. Donner, and T. Esslinger, Cavity optomechanics with a Bose-Einstein condensate, Science **322**, 235 (2008).

[58] G. M. Kavoulakis, Bose-Einstein condensates with attractive interactions on a ring, Phys. Rev. A **67**, 011601(R) (2003).

[59] J. Brand and W. P. Reinhardt, Generating ring currents, solitons and vortices by stirring a Bose–Einstein condensate in a toroidal trap, J. Phys. B: At. Mol. Opt. Phys. **34**, L113 (2001).

[60] L. A. Toikka, O. Kärki, and K.-A. Suominen, Creation and revival of ring dark solitons in an annular Bose–Einstein condensate, J. Phys. B: At. Mol. Opt. Phys. **47**, 021002 (2014).

[61] G. D. McDonald, C. C. N. Kuhn, K. S. Hardman, S. Bennetts, P. J. Everitt, P. A. Altin, J. E. Debs, J. D. Close, and N. P. Robins, Bright solitonic matter-wave interferometer, Phys. Rev. Lett. **113**, 013002 (2014).

[62] J. L. Helm, S. L. Cornish, and S. A. Gardiner, Sagnac interferometry using bright matter-wave solitons, Phys. Rev. Lett. **114**, 134101 (2015).

[63] D. Gallucci and N. P. Proukakis, Engineering dark solitary waves in ring-trap Bose–Einstein condensates, New J. Phys. **18**, 025004 (2016).

[64] D. M. Jezek, P. Capuzzi, and H. M. Cataldo, Dark-soliton collisions in a toroidal Bose-Einstein condensate, Phys. Rev. A **93**, 023601 (2016).

[65] H. Cataldo and D. M. Jezek, Collisional dynamics of multiple dark solitons in a toroidal Bose-Einstein condensate: Quasiparticle picture, Eur. Phys. J. D **72**, 213 (2018).

[66] D. Naidoo, K. Aït-Ameur, M. Brunel, and A. Forbes, Observation of superfluid flow in a Bose-Einstein condensed gas, Appl. Phys. B **106**, 683 (2012).

[67] H. Stoof, Coherent versus incoherent dynamics during Bose-Einstein condensation in atomic gases, J. Low Temp. Phys. **114**, 11 (1999).

[68] H. Stoof and M. Bijlsma, Dynamics of fluctuating Bose–Einstein condensates, J. Low Temp. Phys. **124**, 431 (2001).

[69] P. B. Blakie, A. Bradley, M. Davis, R. Ballagh, and C. Gardiner, Dynamics and statistical mechanics of ultra-cold Bose gases using c-field techniques, Adv. Phys. **57**, 363 (2008).

[70] T. Mithun, S. C. Ganguli, P. Raychaudhuri, and B. Dey, Signatures of two-step impurity-mediated vortex lattice melting in Bose-Einstein condensates, Europhys. Lett. **123**, 20004 (2018).

[71] R. Kubo, The fluctuation-dissipation theorem, Rep. Prog. Phys. **29**, 255 (1966).

[72] S. Ritter, F. Brennecke, K. Baumann, T. Donner, C. Guerlin, and T. Esslinger, Dynamical coupling between a Bose-Einstein condensate and a cavity optical lattice, Appl. Phys. B **95**, 213 (2009).

[73] C. F. Brennecke, Collective interaction between a Bose-Einstein condensate and a coherent few-photon field, Ph.D. thesis, Swiss Federal Institute of Technology, Zurich, 2009.

[74] D. Tan and Z. Chen, On a general formula of fourth order Runge-Kutta method, J. Math. Sci. Mat. Educ. **7**, 1 (2012).

[75] W. Bao, D. Jaksch, and P. A. Markowich, Numerical solution of the Gross–Pitaevskii equation for Bose-Einstein condensation, J. Comput. Phys. **187**, 318 (2003).

[76] R. Kanamoto, H. Saito, and M. Ueda, Stability of the quantized circulation of an attractive Bose-Einstein condensate in a rotating torus, Phys. Rev. A **68**, 043619 (2003).

[77] D. W. Hallwood, T. Ernst, and J. Brand, Robust mesoscopic superposition of strongly correlated ultracold atoms, Phys. Rev. A **82**, 063623 (2010).

[78] M. F. Andersen, C. Ryu, P. Cladé, V. Natarajan, A. Vaziri, K. Helmerson, and W. D. Phillips, Quantized rotation of atoms from photons with orbital angular momentum, Phys. Rev. Lett. **97**, 170406 (2006).

[79] K. Wright, L. S. Leslie, and N. P. Bigelow, Optical control of the internal and external angular momentum of a Bose-Einstein condensate, Phys. Rev. A **77**, 041601(R) (2008).

[80] K. C. Wright, L. S. Leslie, A. Hansen, and N. P. Bigelow, Sculpting the vortex state of a spinor BEC, Phys. Rev. Lett. **102**, 030405 (2009).

[81] C. J. Pethick and H. Smith, *Bose-Einstein Condensation in Dilute Gases* (Cambridge University Press, Cambridge, United Kingdom, 2008).

[82] P. A. Ruprecht, M. J. Holland, K. Burnett, and M. Edwards, Time-dependent solution of the nonlinear Schrödinger equation for Bose-condensed trapped neutral atoms, Phys. Rev. A **51**, 4704 (1995).

[83] V. M. Pérez-García, H. Michinel, and H. Herrero, Bose-Einstein solitons in highly asymmetric traps, Phys. Rev. A **57**, 3837 (1998).

[84] L. Khaykovich, F. Schreck, G. Ferrari, T. Bourdel, J. Cubizolles, L. D. Carr, Y. Castin, and C. Salomon, Formation of a matter-wave bright soliton, Science **296**, 1290 (2002).

[85] K. E. Strecker, G. B. Partridge, A. Truscott, and R. G. Hulet, Formation and propagation of matter-wave soliton trains, Nature (London) **417**, 150 (2002).

[86] S. L. Cornish, S. T. Thompson, and C. E. Wieman, Formation of bright matter-wave solitons during the collapse of attractive Bose-Einstein condensates, Phys. Rev. Lett. **96**, 170401 (2006).

[87] A. L. Marchant, T. P. Billam, T. P. Wiles, M. M. H. Yu, S. A. Gardiner, and S. L. Cornish, Controlled formation and reflection of a bright solitary matter-wave, Nat. Commun. **4**, 1865 (2013).

[88] P. Medley, M. A. Minar, N. C. Cizek, D. Berryrieser, and M. A. Kasevich, Evaporative production of bright atomic solitons, Phys. Rev. Lett. **112**, 060401 (2014).

[89] S. Lepoutre, L. Fouché, A. Boissé, G. Berthet, G. Salomon, A. Aspect, and T. Bourdel, Production of strongly bound ^{39}K bright solitons, Phys. Rev. A **94**, 053626 (2016).

[90] T. Mežnaršič, T. Arh, J. Brence, J. Pišljar, K. Gosar, Ž. Gosar, R. Zitko, E. Zupanič, P. Jeglič *et al.*, Cesium bright matter-wave solitons and soliton trains, Phys. Rev. A **99**, 033625 (2019).

[91] K. Furutani and L. Salasnich, Superfluid properties of bright solitons in a ring, Phys. Rev. A **105**, 033320 (2022).

[92] H. Saito and R. Kanamoto, Self-rotation and synchronization in exciton-polariton condensates, Phys. Rev. B **94**, 165306 (2016).

[93] S. Gardiner, K. Gheri, and P. Zoller, Cavity-assisted quasiparticle damping in a Bose-Einstein condensate, Phys. Rev. A **63**, 051603(R) (2001).

[94] A. Ali, F. Saif, and H. Saito, Phase separation and multistability of a two-component Bose-Einstein condensate in an optical cavity, Phys. Rev. A **105**, 063318 (2022).